

SYNTHESIS AND MAGNETIC CHARACTERIZATION OF Mn-Ti SUBSTITUTED $\text{SrO} \cdot 0.6\text{Fe}_{2-x}\text{Mn}_{x/2}\text{Ti}_{x/2}\text{O}_3$ ($x = 0.0-1.0$) NANOPARTICLES BY COMBINED DESTRUCTION PROCESS

Karina Nur Fitriana¹, Mas Ayu Elita Hafizah¹, Azwar Manaf^{1*}

¹*Material Science Study, Physics Department, Faculty of Mathematics and Natural Sciences,
Universitas Indonesia, Jl. Salemba Raya No. 4, Jakarta 10430, Indonesia*

(Received: January 2017 / Revised: March 2017 / Accepted: June 2017)

ABSTRACT

Single phased $\text{SrO} \cdot 0.6\text{Fe}_{2-x}\text{Mn}_{x/2}\text{Ti}_{x/2}\text{O}_3$ ($x = 0.0; 0.5; \text{ and } 1.0$) nanoparticles, whose mean size was comparable with the crystallite size, were successfully fabricated through mechanical alloying and a subsequent ultrasonic destruction processes. The ultrasonic destruction process employed a transducer operated under amplitudes of 35, 45, and 55 μm . Results indicated that the mean particle size was not determined by the transducer amplitude, but the mechanical properties of the materials, as well as the initial size of the particles. After ultrasonic destruction, the mean sizes of the particles decreased to the range of 87–194 nm with a narrow distribution width. The mean particle sizes were about 1 to 3 times larger than the respective crystallite sizes. Such fine particles were aimed to decrease the coercivity, as was seen in the sample with $x = 0$, which showed a decrease in coercivity from $474 \text{ kA} \cdot \text{m}^{-1}$ to $24 \text{ kA} \cdot \text{m}^{-1}$ and $15 \text{ kA} \cdot \text{m}^{-1}$. A further reduction in the coercivity was observed in Mn-Ti substituted strontium hexaferrite.

Keywords: Mechanical alloying; Nanoparticle; Sonochemistry; Strontium hexaferrite; Ultrasonic destruction

1. INTRODUCTION

The synthesis and characterization of nanoparticles represent a major development in materials research because of the fascinating size-dependent properties and wide range of applications of nanoparticles (Banasadi et al., 2014; Cullity & Graham, 2008). Nanotechnology has therefore been the most interesting research topic for scientists thus far (Tabatabaie et al., 2009). Moreover, the impacts of the benefits of nanotechnology are greater at the industrial level. The production of nanosized materials with the required characteristics and specific purposes has resulted in the miniaturization of products such as headphones and computers that not only exhibit significantly reduced dimensions but also maintain optimal performance.

In magnetism applications, strontium hexaferrite (SHF) is a well-known and widely used permanent magnet (Cullity & Graham, 2008), because it meets all requirements of such application. It has a large total magnetization value ($M_s = 0.48 \text{ T}$) with a high Curie temperature ($T_c = 723 \text{ K}$) and a large magnetocrystalline constant ($H_A = 3.3 \times 10^5 \text{ J} \cdot \text{m}^{-3}$) (Cullity & Graham, 2008). In addition, SHF is a chemically stable material because it is an oxide-based compound hence resistant to change of its properties. Structural modification of

*Corresponding author's email: azwar@ui.ac.id, Tel. +62-21-786-2610, Fax. +62-21-786-3441
Permalink/DOI: <https://doi.org/10.14716/ijtech.v8i4.7388>

SHF through Mn-Ti substitution has showed the ability of absorbing microwaves, which can reduce interference of electromagnetic waves (Baniasadi et al., 2014; Jamalian et al., 2014). Unfortunately, the coercivity of SHF is very high ($H_c \approx 250 \text{ kA.m}^{-1}$), and hence, it needs a very high resonance frequency ($f_r = 13.4\text{--}19.4 \text{ GHz}$) (Ataie, 2001; Baniasadi et al., 2014; Jamalian et al., 2014; Manawan et al., 2014; Tabatabaie et al., 2009). However, the high coercivity could be reduced so that it would be useful in most applications like RADAR.

One way to reduce the coercivity of SHF is by partially substituting the Fe ion in SHF by Mn-Ti ions, which would result in a decrease in the magnetocrystalline constant and the total magnetization values. The high coercivities of SHF can be reduced by allowing the grain exchanged interaction effect (Hadjipanayis & Prinz, 1991; Jamalian et al., 2014) to take place. Therefore, synthesis of $\text{SrO.6(Fe,Mn,Ti)}_2\text{O}_3$ nanoparticles is essential. The composition of dopants and the size of particles have been shown to affect the magnetic properties of Mn-Ti substituted strontium hexaferrite (Manawan et al., 2014; Mozaffari et al., 2010). Moreover, an effective fabrication process also contributes to the formation of nanoparticles. A mechanical alloying process, which involves the ultrasonic destruction of mechanically milled powder, would be an alternative method for the fabrication of nanoparticles. In the ultrasonic destruction process, the amplitude of the transducer would control the power that forms the cavitation or the nucleation of cavities (Baniasadi et al., 2014; Merouani et al., 2014). In this paper, results of the particle and crystallite size evaluations of Mn-Ti substituted SHF are discussed. The particles were synthesized through a mechanical alloying combined with the ultrasonic destruction process, employed a transducer operated under various transducer amplitude values. The implications of the partial ionic substitution effect on the magnetic properties of Mn-Ti substituted SHF nanoparticles based material is also reported.

2. METHODOLOGY

Nanoparticles for samples of $\text{SrO.6Fe}_{2-x}\text{Mn}_{x/2}\text{Ti}_{x/2}\text{O}_3$ ($x = 0.0; 0.5; \text{ and } 1.0$) compositions were first synthesized through a mechanical alloying method. Stoichiometry quantities of analytical-grade SrCO_3 , Fe_2O_3 , MnCO_3 , and TiO_2 precursors with a purity greater than 99 wt.% were mixed and milled using a planetary ball mill to a powder weight ratio of 10:1. Powders obtained after 20 h of milling were assumed to be highly deformed materials. The sintered samples were prepared by consolidating mechanically alloyed powders into a metal die and subsequently pressed into a green compact prior to sintering. The sintering temperature was 1200°C for 3 h to form crystalline materials. The sintered samples were then re-milled for 10 h to obtain fine crystalline particles.

Three grams of each of the crystalline particles were dispersed in 97 ml of aquabidest, and then, these were subjected to an ultrasonic destruction treatment for 5 h using a transducer operated at amplitude of 35, 45, and 55 μm , respectively. Dispersion containing the particles were dried at a temperature of 150°C to obtain fine powders. The particle sizes were evaluated by a Malvern Zetasizer Nano system, whereas the crystallite size was analyzed by PM2K software, whose fitting was based on the WPPM method. The fitting data were determined from the results of the XRD data refinement. The magnetic properties were evaluated by a hysteresisgraph, particularly for hard magnetic materials (PERMAGRAPH[®] L MAGNET-PHYSIK Dr.Steingroever GmbH).

3. RESULTS AND DISCUSSION

3.1. Effect of Transducer Amplitude on the Particles and Crystallites in Ultrasonic Destruction Process

The XRD diffraction patterns of the three samples ($x = 0$; 0.5 and 1.0) generally remain similar, but there is some shift in the peak positions. Figure 1 compares the XRD plot for $x = 0$ with those for $x = 0.5$ and 1.0 in the diffraction angle range of $25^\circ-60^\circ$. An insignificant shift in all the peak positions can be seen in this range. This shift is due to a difference in the ionic radii of the dopant, in which the ionic radii of Mn^{2+} (0.80 Å) is larger than that of Fe^{3+} (0.63 Å) (Shannon, 1976). Consequently, the cell dimension also changed with the composition, i.e., for samples with $x = 0.5$ and 1.0, the change in cell volume was 0.7% and 2.6%, respectively, greater than that of $x = 0$. Mn-Ti ions occupy the site of Fe ions at Fe1, Fe2, and Fe5 (2a, 2b, and 12k), and thus, the intensity of some peaks significantly changed like those of (006) and (008) (Baniasadi et al., 2014; Hadjipanayis & Prinz, 1991; Jamalians et al., 2014). It is because index (00 l) has different reflection condition according to the refinement of diffraction pattern. As SHF has hexagonal crystal structure and thus one of the lattice parameter is bigger ($a = b \neq c$). In this regard, different calculation may occur for particular index where it follows c -planes (Dunne et al., 2012). Figure 1 shows peaks of the (110) and (116) planes especially, which belonged to the SHF phase as the parent phase for these samples. These peaks are not shown in $x = 0$, since although they were present, they had a very low intensity (quantitatively only about 3%).

As a result, they were not included while refining the diffraction pattern using the WPPM method, which usually presents peaks with predominantly high intensity (Scardi & Leoni, 2002).

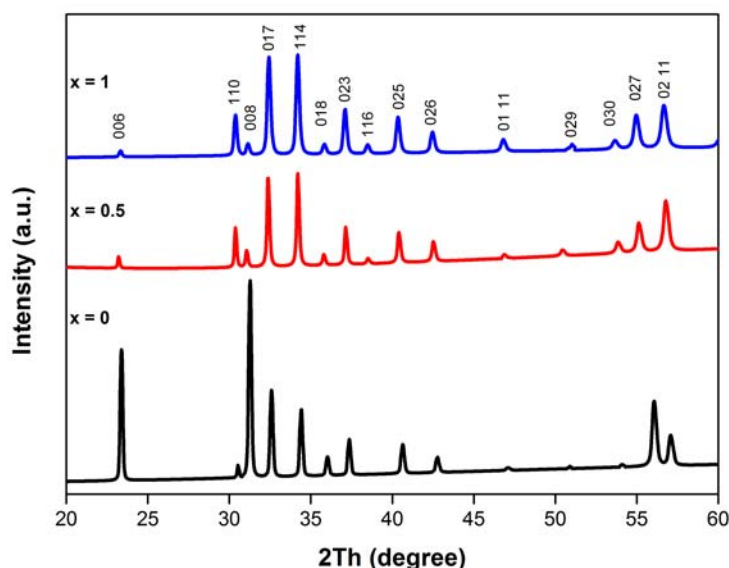


Figure 1 Plot of diffraction peaks of SHF ($x = 0$) in diffraction angle range of $20^\circ-60^\circ$ compared with those that of Mn-Ti substituted SHF ($x = 0.5$ and 1.0)

Plots of the mean crystallite size of $\text{SrO} \cdot 6\text{Fe}_{2-x}\text{Mn}_{x/2}\text{Ti}_{x/2}\text{O}_3$ ($x = 0.0$; 0.5; and 1.0) samples, which compared with their respective mean particle size obtained from ultrasonic treatment using transducer operated at three different amplitudes were presented in Figure 2. The crystallite size was obtained through XRD data evaluation using the WPPM method (Scardi & Leoni, 2002). In this method, various microstructural details are required to be evaluated along with other parameters like the instrumental broadening, crystal structure, lattice parameters. In addition, a distribution function like the average lognormal distribution was involved in the

evaluation of crystallite size. This size parameter will affect the size distribution through the lognormal distribution approach (see Figure 2d) which uses the Fourier transform of the only expanded size profile. Furthermore, crystal defects and faulting effects are also considered during the expansion of the diffraction lines. Therefore, this method is appropriate for evaluating the heavy deformed samples obtained by the destruction process (Scardi & Leoni, 2002; Mittemeijer & Welzel, 2008).

Of the three plots in Figure 2, it showed that the magnitude of the transducer amplitude determines the decrease of particle size, although the difference between the three is not much different. Only transducer with amplitude of 55 μm , which takes in the most significant reduction. Particularly, in sample with $x = 0$, the ultrasonic treatment resulted in mono-crystallite particles. The particle size distribution for this sample is plotted in Figure 2d, from which it depicts the size of particles in the range 76–94 nm with a mean size 84 nm. It is a narrow size distribution attributed a sample with homogenous mono-crystallite particles. While for substituted SHF samples ($x = 0.5$ and 1.0), both particle and crystal size were also reduced, although not significantly. Hence, samples still contained multi-crystallite particles. It is assured that the ultrasonic treatment for reduction of particle and crystallite size, the use of a transducer with amplitude of 55 μm was found to be more effective in reducing the particle size.

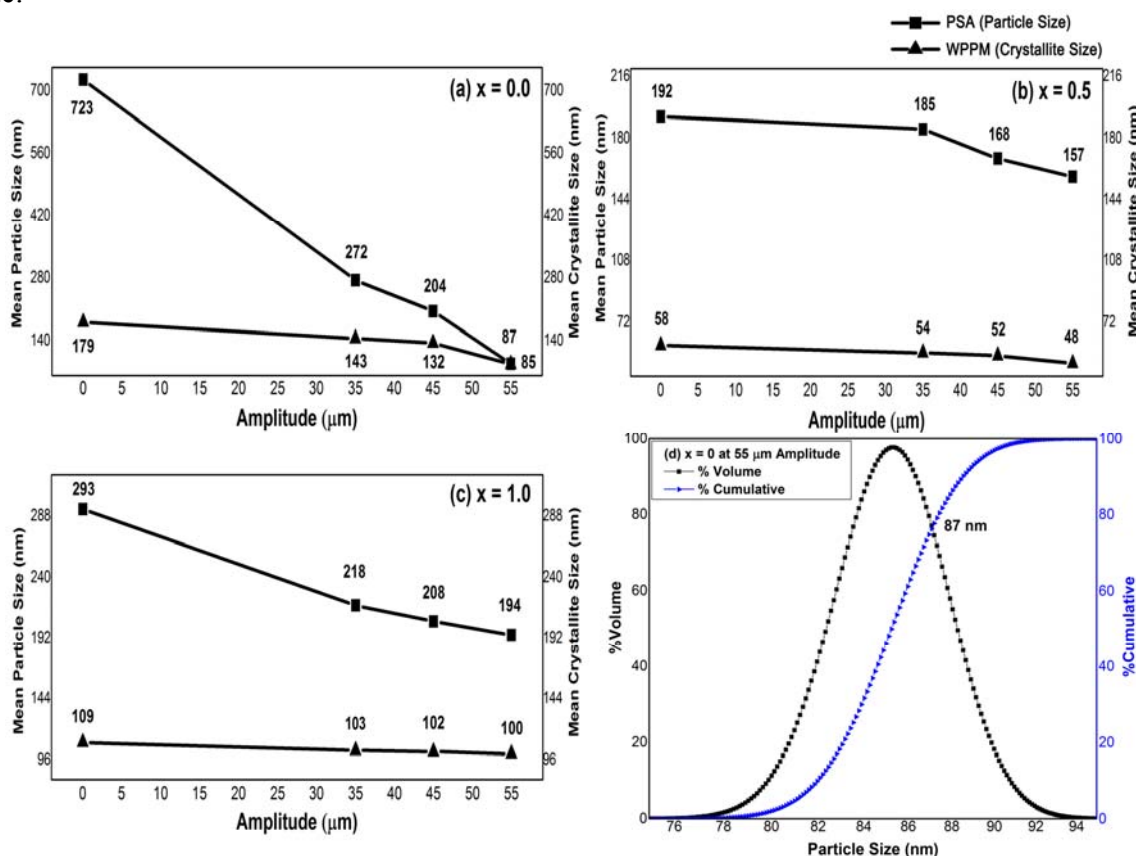


Figure 2 Plot of mean particle and crystallite size for samples of: (a) $x = 0$; (b) $x = 0.5$; (c) $x = 1.0$ before and after ultrasonic treatment; and (d) particle size distribution for monocrystalline particles after ultrasonic treatment under amplitude of 55 μm .

Results as summarized in Figure 2 suggest that the fragmentation of crystals is still possible by the ultrasonic destructor if the crystal size is relatively large. The employment of transducer with an increased amplitude has a linear trend line with transducer power, which generated cavitation with different effects. This effect is specifically towards the bubbles that are

conducted by the transducer. Due to the increasing of transducer power, hence the bubbles collapse more intensive along with SHF sample (Merouani et al., 2014). Results in Figures 2a, 2b, and 2c show that the crystallites in dopant-containing particles were smaller than those in dopant-free particles. However, all particles that received ultrasonic treatment had particle size that was about twice the crystallite size. It is also indicated that the particle size of the dopant-containing particle is more ductile rather than dopant-free particle, because it is not easily reduced through this second destruction process. Apart from the sample with $x = 0$, sample with $x = 0.5$ and 1.0 had monocrystalline particles after the ultrasonic treatment. As shown in Figure 2(d), all particles were below 95 nm after the second process under $55 \mu\text{m}$ amplitude for the unsubstituted SHF, which had a mean particle size of 87 nm . According to the cumulative curve, this particle size is particularly obtained approximately during the 80% of the second process. Also from this curve (Figure 2d), it shows that the particle size through $55 \mu\text{m}$ amplitude to $x = 0$ has quite rapid reduction since it reduced within the small range of particle size ($76-94 \text{ nm}$).

3.2. Magnetic Properties

The effect of nanostructured material on the magnetic properties of SHF is shown in Figure 3, which compares hysteresis loops. The hysteresis loop of SHF is typical of permanent magnets with relatively large coercivities of more than $400 \text{ kA} \cdot \text{m}^{-1}$, as has also been reported by Ataie et al. ($445 \text{ kA} \cdot \text{m}^{-1}$) (Ataie, 2001). However, the coercivity reduced very significantly when the crystallite size was in the range of $85-143 \text{ nm}$, in which each amplitude alteration corresponds to particle and crystallite size, as presented in Figure 2a. This reduction was also followed by an insignificant decrease in the remanent magnetization. The reduction in coercivity can be attributed to the grain exchange interaction effect, as has been reported in the literature (Hadjipanayis & Prinz, 1991) to occur in nanocrystalline magnetic materials.

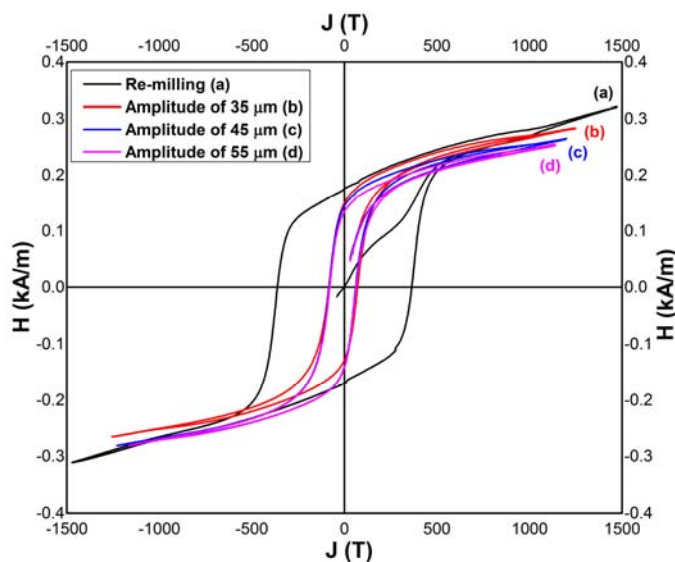


Figure 3 Second quadrant of hysteresis loop for sample $\text{SrO} \cdot 6\text{Fe}_{2-x}\text{Mn}_{x/2}\text{Ti}_{x/2}\text{O}_3$ $x = 0$ shows the effect of fine crystallite size on the coercivity with respect to transducer amplitude: (a) Re-milled sample (amplitude of $0 \mu\text{m}$); (b) amplitude of $35 \mu\text{m}$; (c) amplitude of $45 \mu\text{m}$; and (d) amplitude of $55 \mu\text{m}$

The presence of Mn-Ti ions with substituted iron in a 2b site causes reduction of the magnetocrystalline anisotropy constant for the magnetic SHF phase (Hadjipanayis & Prinz, 1991; Manawan et al., 2014; Tabatabaie et al., 2009). This site is assigned to be one of the sites for providing the large anisotropy field (Manawan et al., 2014), and hence, H_c would be reduced. A strong uniaxial anisotropy is along the c-axis, which belongs to easy axis

magnetization, and it later changes to c-plane (Manawan et al., 2014). The further decreasing coercivity value is altered with increasing x , which indicates changes in properties. The quantitative result of the hysteresis loop shows that the coercivity of the re-milled sample decreased from $474 \text{ kA}\cdot\text{m}^{-1}$ to $24 \text{ kA}\cdot\text{m}^{-1}$ owing to ionic substitution. This is accompanied with a decrease in the remanence value.

A very low coercivity value of Mn-Ti substituted SHF is believed to be due to the combined effect of the low magnetocrystalline constant and the nanocrystalline structure. The decreased value of remanent magnetization observed in the dopant-containing samples is not in agreement with most reports on the grain exchanged interaction effect in magnetic materials, in which a reduction in coercivity is followed by an increase in the remanent magnetization (Hadjipanayis & Prinz, 1991; Jamalain et al., 2014). Furthermore, based on research, this decrease in coercivity could be also supported by the extrinsic effect of increasing particle size (as shown in Figures 2a, 2b, and 2c) and intergranular network with substitution (Manawan et al., 2014). We believe that, in the current case, the lower remanence value was primarily due to the presence of porosity because the mass density of the sample was found to be a bit low.

4. CONCLUSION

Materials of $\text{SrO}\cdot 6\text{Fe}_{2-x}\text{Mn}_{x/2}\text{Ti}_{x/2}\text{O}_3$ ($x = 0, 0.5, \text{ and } 1.0$) compositions were synthesized through mechanical alloying, and were identified as single phase materials. Prior to ultrasonic treatment, the mechanically milled particles exhibited a broad size distribution, with particle sizes of up to 700 nm. After ultrasonic treatment, the particle sizes progressively reduced. Ultrasonic destruction process with $55 \mu\text{m}$ transducer amplitude was found to be effective in obtaining monocrystalline particles with sizes up to ~ 87 nm. The effect of the nanostructure in the material significantly reduced the coercivity. In the case of dopant-free SHF, the coercivity of $474 \text{ kA}\cdot\text{m}^{-1}$ reduced to $24 \text{ kA}\cdot\text{m}^{-1}$ after the particle sizes reduced to 87 nm. In addition, a much lower reduction in coercivity occurred when Fe ions in SHF were partially replaced by Mn-Ti ions.

5. ACKNOWLEDGEMENT

The authors gratefully acknowledge the support of Physics Department University of Indonesia for the research facilities. We are also thankful for the financial support provided by the university under the research grant contract no. 1861/UN2.R12/HKP 05.00/2015.

6. REFERENCES

- Ataie, A., 2001. Synthesis of Ultra-fine Particles of Strontium Hexaferrite by a Modified Coprecipitation Method. *Journal of European Ceramic Society*, Volume 21, pp. 1951–1955
- Baniasadi, A., Ghasemi, A., Nemati, A., Azami Ghadikolaei, M., Paimozd, E., 2014. Effect of Ti-Zn Substitution on Structural, Magnetic and Microwave Absorption Characteristics of Strontium Hexaferrite. *Journal of Alloys and Compounds*, Volume 583, pp. 325–328
- Cullity, B.D., Graham, C.D., 2008. *Introduction to Magnetic Materials*. New Jersey: John Wiley & Sons, Inc.
- Dunne, F.P.E., Kiwanuka, R., Wilkinson, A.J., 2012. Crystal Plasticity Analysis of Microdeformation, Lattice Rotation and Geometrically Necessary Dislocation Density. *In: Proceedings of The Royal Society A: Mathematical, Physical, and Engineering Sciences*, Volume 468(2145), pp. 2509–2531
- Hadjipanayis, G.C., Prinz, G., 1991. Science and Technology of Nanostructured Magnetic Materials. (Hadjipanayis, G.C.; Prinz, G., Ed.), *In: Nato Science Series B: Physics* (1st ed.). Springer US, USA

- Jamalian, M., Ghasemi, A., Paimozd, E., 2014. Sol-Gel Synthesis of Mn-Sn-Ti-Substituted Strontium Hexaferrite Nanoparticles: Structural, Magnetic, and Reflection-loss Properties. *Journal of Electronic Materials*, Volume 43(4), pp. 1076–1082
- Manawan, M., Manaf, A., Soegijono, B., Yudi, A., 2014. Microstructural and Magnetic Properties of Ti^{2+} - Mn^{4+} Substituted Barium Hexaferrite. *Advanced Materials Research*, Volume 896, pp. 401–405
- Merouani, S., Hamdaoui, O., Rezgui, Y., Guemini, M., 2014. Energy Analysis during Acoustic Bubble Oscillation: Relationship between Bubble Energy and Sonochemical Parameters. *Ultrasonics*, Volume 54(1), pp. 227–232
- Mittemeijer, E.J., Welzel U., 2008. The "State of Art" of Diffraction Analysis of Crystallite Size and Lattice Strain. *Zeitschrift für Kristallographie*, Volume 223, pp. 552–560
- Mozaffari, M., Arab, A., Yousefi, M. H., Amighian, J., 2010. Preparation and Investigation of Magnetic Properties of MnNiTi-Substituted Strontium Hexaferrite Nanoparticles. *Journal of Magnetism and Magnetic Materials*, Volume 322(18), pp. 2670–2674
- Scardi, P., Leoni, M., 2002. Whole Powder Pattern Modelling. *Acta Crystallographica Section A: Foundations of Crystallography*, Volume 58(2), pp. 190–200
- Shannon, R.D., 1976. Revised Effective Ionic Radii and Systematic Studies of Interatomic Distances in Halides and Chalcogenides. *Acta Crystallographica*, Volume A32, pp. 751–767
- Tabatabaie, F., Fathi, M.H., Saatchi, A., Ghasemi, A., 2009. Microwave Absorption Properties of Mn- and Ti-doped Strontium Hexaferrite. *Journal of Alloys and Compounds*, Volume 470(1–2), pp. 332–335